

# Enhancing dark siren cosmology through multi-band gravitational wave synergetic observations

Yue-Yan Dong,<sup>1,\*</sup> Ji-Yu Song,<sup>1,\*</sup> Shang-Jie Jin,<sup>1,2</sup> Jing-Fei Zhang,<sup>1</sup> and Xin Zhang<sup>1,3,4,†</sup>

<sup>1</sup>*Key Laboratory of Cosmology and Astrophysics (Liaoning) & College of Sciences, Northeastern University, Shenyang 110819, China*

<sup>2</sup>*Department of Physics, University of Western Australia, Perth WA 6009, Australia*

<sup>3</sup>*Key Laboratory of Data Analytics and Optimization for Smart Industry (Ministry of Education), Northeastern University, Shenyang 110819, China*

<sup>4</sup>*National Frontiers Science Center for Industrial Intelligence and Systems Optimization, Northeastern University, Shenyang 110819, China*

Multi-band gravitational-wave (GW) standard siren observations are poised to herald a new era in the study of cosmic evolution. These observations offer higher signal-to-noise ratios and improved localizations compared to those achieved with single-band GW detection, which are crucial for the cosmological applications of dark sirens. In this work, we explore the role multi-band GW synergetic observations will play in measuring cosmological parameters, particularly in comparison with single GW observatory data. We used mock multi-band dark siren data from third-generation GW detectors and the baseline Decihertz Interferometer Gravitational-Wave Observatory to infer cosmological parameters. Our analysis was conservative, involving only the 89 actual GW events from the current Gravitational Wave Transient Catalogs in our data simulation, facilitating a direct comparison with existing dark siren results. Multi-band GW observations significantly improve sky localization accuracy by two to three orders of magnitude over single-band observations, although their impact on luminosity distance error remains limited. This results in a substantial improvement in the constraints on matter density and the Hubble constant, enhancing them by 75% to 85% and 65% to 82%, respectively. We conclude that the significant potential of multi-band GW synergistic observations for detecting GW signals and resolving the Hubble tension is highly promising and warrants anticipation.

## I. INTRODUCTION

The Hubble tension has emerged as a significant enigma in cosmology in recent years [1–6]. This confusion stems from a more-than- $5\sigma$  discrepancy between the values of the Hubble constant ( $H_0$ ) inferred from the Planck 2018 CMB observation [7] based on the  $\Lambda$ CDM model (a 0.8% measurement) and obtained through the model-independent distance ladder measurement (a 1.4% measurement) [8]. This inconsistency hints at the possibility of new physics beyond the  $\Lambda$ CDM model (see, e.g., Refs. [9–36]). However, no consensus is reached on a valid extended cosmological model that can truly resolve the Hubble tension [17]. Therefore, one may pay more attention to some promising and powerful cosmological probes that can independently measure  $H_0$  to help resolve the Hubble tension. The gravitation wave (GW) standard sirens are a promising new cosmological probe that could help determine the  $H_0$  value independently, which is widely discussed in Refs. [37–86] and references therein.

Compact binary coalescence (CBC) events produce GWs whose waveforms encode the luminosity distance information. Through the GW waveform analysis, one can

directly obtain the luminosity distance, which is vividly referred to as a standard siren [87, 88]. Once the redshifts of GW sources are determined, the established distance-redshift relation can be used to explore the cosmic expansion history. There are mainly two methods regarding the redshift determinations of GW sources adopted by the current GW observations. One is to determine redshift through its electromagnetic (EM) counterparts, an event that relies on the binary neutron star (BNS) merger (usually referred to as a bright siren). The other is to use the cross-correlation between GW localization and galaxy catalog, inferring the redshift through a statistical method (usually referred to as a dark siren) [84, 89–105].

So far, the first, second, and third observation runs from the LIGO-Virgo-KAGRA (LVK) collaboration have reported over 90 CBC events [106–108]. However, owing to the challenge in detecting EM counterparts, only one bright siren, GW170817, has been identified, which yields approximately a 14% constraint on  $H_0$  [109]. For dark siren analysis, using 46 dark siren events with SNRs over 11, combined with the GLADE+ catalog [110, 111], achieves a 19% constraint on  $H_0$  [101, 112]. Additionally, the 46 dark sirens combined with the one bright siren GW170817 constrain  $H_0$  to around 10% [101], which have not yet reached the level required to resolve the Hubble tension.

In the future, the multi-band relay detection of a GW event becomes possible. In the hectohertz to kilohertz band, the cutting-edge third-generation (3G) ground-based GW detectors, i.e., the Einstein Telescope (ET)

\*These authors contributed equally to this paper.

†Corresponding author.

zhangxin@mail.neu.edu.cn

[113] and the Cosmic Explorer (CE) [114], are set to debut, anticipated to achieve sensitivity enhancements by an order of magnitude than current GW detectors. The space-based baseline Decihertz Interferometer Gravitational-Wave Observatory (B-DECIGO) with longer arms will provide a detection window in the decihertz band. In addition, GW signals in the millihertz band will be detected by space-based GW detectors with even longer arms, such as LISA [115–117], Taiji [118–120], and TianQin [121–126]. The concept of the multi-band GW observations has been widely investigated in Refs. [127–146], and several advantages are dug out: providing early warnings of the detection of BNSs, which is crucial of EM counterparts searches; enhancing the accumulation of signal-to-noise (SNR); improving the precisions of GW parameters inference, including the spatial localization precision.

We notice the current dark sirens analysis with GWTC-3 and GLADE+ catalog has very poor localization, with sky localization primarily a few hundred square degrees, occasionally extending to a few thousand, and high luminosity distance measurement errors, ranging from 40 Mpc to several thousands of Mpc at the  $1\sigma$  level. We anticipate in the future, using the multi-band synergetic detection of the GW events will substantially enhance spatial localization precision, thereby improving the precision of constraints on cosmological parameters with dark sirens. Therefore, we wish to study how multi-band synergetic detection of GW events enhances the dark siren cosmology.

In this work, we simulate the multi-band synergetic detection of B-DECIGO and 3G ground-based GW detectors for 89 GW events from GWTC-3 that lack EM counterparts. Then, we constrain cosmological parameters in the  $\Lambda$ CDM model. The synergy of B-DECIGO and 3G GW ground-based detectors is particularly well-suited for detecting stellar-mass binary black hole (SBBH) merger events, and by using the same GW event catalog, we can compare our results with the current actual dark siren analysis and explore how multi-band GW synergetic detection enhances the cosmological constraint precisions with dark sirens in detail. It is worth noting that from the up-to-date inference with GWTC-3, the merger rate of SBBH is  $23.9_{-8.6}^{+14.9} \text{ Gpc}^{-3} \text{ yr}^{-1}$  [147], and hence we can roughly forecast the SBBH detection rate of B-DECIGO and 3G ground-based detectors, which is far higher than current detection using LVK. Therefore, in the future, when our multi-band GW synergetic observation strategy can be implemented, there will be a large number of dark siren events that can be used for cosmological parameter inference, and the accuracy will be much higher than that envisioned in this paper. We once again emphasize that this paper only considers 89 GW events (corresponding to the currently actually observed events), because this allows us to compare the results we obtain with the current actual single-band observation results, thereby highlighting the great advantages of implementing a multi-band synergetic observation strategy in cosmological parame-

ter inference.

This paper is organized as follows. In Sec. II, we introduce the methods of simulating the multi-band synergetic detection GW data and the dark siren analysis. In Sec. III, we give the constraint results and make detailed discussions. The conclusion is given in Sec. IV.

## II. METHOD

### A. Cosmological model

In the expanding universe, the luminosity distance  $d_L$  can be expressed theoretically as

$$d_L(z) = c(1+z) \int_0^z \frac{dz'}{H(z')}, \quad (1)$$

where  $c$  is the speed of light in vacuum, and  $H(z)$  is the Hubble parameter, describing the universe's expansion rate at redshift  $z$ .

In the standard model of cosmology, the  $\Lambda$ CDM model, the equation of state parameter of dark energy  $w = -1$ , and  $H(z)$  can be expressed as

$$H(z) = H_0 \sqrt{\Omega_m(1+z)^3 + 1 - \Omega_m}. \quad (2)$$

In our GW data simulation, we adopt the  $\Lambda$ CDM model as the fiducial model with  $H_0 = 67.27 \text{ km s}^{-1} \text{ Mpc}^{-1}$  and  $\Omega_m = 0.3166$  from the constraint results of Planck 2018 TT, TE, EE+lowE [7].

### B. GW standard sirens

For a GW detector network composed of  $N$  GW detectors, the Fourier transform of the time-domain waveform is given by [148, 149]

$$\tilde{\mathbf{h}}(f) = e^{-i\Phi} \hat{\mathbf{h}}(f), \quad (3)$$

where  $\Phi$  is a  $N \times N$  diagonal matrix, with  $\Phi_{kl} = 2\pi f \delta_{kl}(\mathbf{n} \cdot \mathbf{r}_k)$ . Here,  $\delta_{kl}$  is the Kronecker delta,  $\mathbf{n}$  is the propagation direction of a GW, and  $\mathbf{r}_k$  represents the location of  $k$ th GW detector.  $\hat{\mathbf{h}}(f)$  is given by

$$\hat{\mathbf{h}}(f) = [\tilde{h}_1(f), \tilde{h}_2(f), \dots, \tilde{h}_N(f)], \quad (4)$$

where  $\tilde{h}_k(f)$  is the frequency-domain GW waveform of  $k$ th GW detector. In this work, we consider the phenomenological non-spinning inspiral-merger-ringdown (IMR) GW model, PhenmonA, to simulate GW signals [150, 151], and calculate the waveform to the 3.5 post-Newtonian (PN) order [152–154].  $\tilde{h}_k$  is given by

$$\tilde{h}_k(f) = \mathcal{A} \sqrt{(F_{+,k}(1 + \cos^2 \iota))^2 + (2F_{\times,k} \cos \iota)^2} e^{i\Psi}, \quad (5)$$

where  $\mathcal{A}$  is the Fourier amplitude. In the PhenmonA model,  $\mathcal{A}$  is expressed as

$$\mathcal{A} = \mathcal{A}_{\text{eff}} \begin{cases} \left(\frac{f}{f_0}\right)^{-7/6}, & f < f_0, \\ \left(\frac{f}{f_0}\right)^{-2/3}, & f_0 \leq f < f_1, \\ \omega \mathcal{L}(f, f_1, f_2), & f_1 \leq f < f_3, \end{cases} \quad (6)$$

and

$$\mathcal{A}_{\text{eff}} = \frac{1}{d_L} \sqrt{\frac{5}{96}} \mathcal{M}_c^{5/6} f_0^{-7/6} \left(\frac{1}{\pi}\right)^{2/3}, \quad (7)$$

where  $f_0$  and  $f_1$  are the beginning frequencies of the merger and the ring-down phases, respectively.  $f_2$  is the decay-width of the ring-down phase, and  $f_3$  is the cut-off frequency of the GW signal.  $M = m_1 + m_2$  is the total mass of the compact binary system, and  $\mathcal{M}_c = \eta^{3/5} M(1+z)$  is the chirp mass, with  $\eta = m_1 m_2 / M^2$  being the symmetric mass ratio. Details of  $\omega$  and  $\mathcal{L}$  can refer to Refs. [116, 150, 151].

$F_{+,k}(f)$  and  $F_{\times,k}(f)$  are antenna response functions of the  $k$ th GW detector, which are related to both the locations of the GW source and the detector. In this work, we analyze ET, two CEs, and B-DECIGO. CE in the USA has 40 km length of arms, denoted as CE (40 km), while the other in Australia with similar design but shortened 20 km length of arms, denoted as CE (20 km). In addition, we include various network configurations. These configurations encompass the 2CE network, consisting of two CEs; the ET2CE network, comprising ET and 2CE; the B-DECIGO-ET network, which combines B-DECIGO and ET; the B-DECIGO-2CE network, involving B-DECIGO and 2CE; and finally, the B-DECIGO-ET2CE network, incorporating B-DECIGO and ET2CE. The specific locations of ground-based GW detectors are referenced in Refs. [155, 156], while the case of B-DECIGO can be found in Ref. [157]. The detailed forms of each GW detector's antenna response function refer to Refs. [158–162].

$\iota$  is the inclination angle in the detector frame and  $\Psi$  is given by

$$\Psi = 2\pi f t_c - \pi/4 + 2\psi(f/2) - \varphi_{(2,0)}. \quad (8)$$

where  $\psi(f)$  and  $\varphi_{(2,0),k}$  are given by Refs. [153, 154]

$$\psi(f) = -\psi_c + \frac{3}{256\eta} \sum_{a=0}^7 \psi_a (2\pi M f)^{(a-5)/3}, \quad (9)$$

$$\varphi_{(2,0),k} = \tan^{-1} \left( -\frac{2 \cos \iota F_{\times,k}}{(1 + \cos^2 \iota) F_{+,k}} \right). \quad (10)$$

### C. Calculation of SNR

The input GW source parameters used for simulating the GW signals are from the 89 compact binaries

collected in GWTC-3 [163], except for GW170817. It is worth noting that the sky positions of GW events in GWTC-3 are represented in the geocentric coordinate system. These positions are subsequently converted to the sky positions in the ecliptic coordinate system when simulating strains of space-based GW detectors. When we simulate the GW detection, we adopt the detection threshold of SNR to be 8. The SNR of the detector network composed of  $N$  GW detectors can be expressed as

$$\rho = \sqrt{\sum_{k=1}^N (\tilde{h}_k | \tilde{h}_k)}, \quad (11)$$

where  $\tilde{h}_k$  is the GW waveform of the  $k$ th GW detector. The inner product is defined as

$$(\tilde{h} | \tilde{h}) = 4 \int_{f_{\text{in}}}^{f_{\text{out}}} \frac{\tilde{h}(f) \tilde{h}^*(f)}{S_n(f)} df, \quad (12)$$

where  $\tilde{h}^*(f)$  is the complex conjugate of  $\tilde{h}(f)$  and  $S_n(f)$  is the one-side noise power spectral density (PSD) of the GW detector. Here we adopt the PSD of ET from Ref. [164], of CE (40 km) from Ref. [165], of CE (20 km) from Ref. [164], and of B-DECIGO from Ref. [129]. Moreover,  $f_{\text{in}}$  and  $f_{\text{out}}$  are the frequencies at which the GW signal enters and leaves the frequency band of the GW detector, respectively.

In Fig. 1, we show the characteristic sensitivities of ET, CE (40 km), CE (20 km), B-DECIGO, LIGO in Livingston and VIRGO (see Ref. [112]). Note that the GW190725-like event is shown as the representative since it has the highest calculated SNR of the multi-band observation among the GW events. It can be found that the frequency band of B-DECIGO is well connected with ground-based detectors, enabling the accumulation of a higher SNR across the longer frequency band.

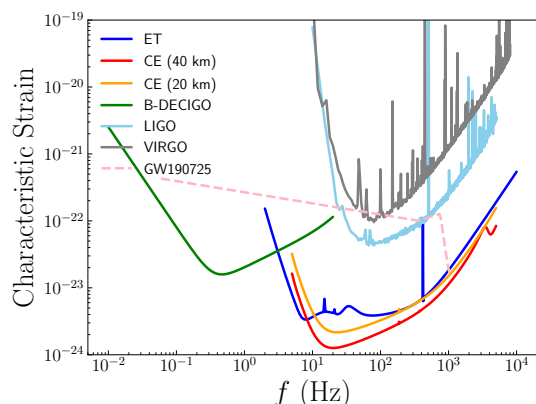


FIG. 1: Characteristic strains of ET, CE (40 km), CE (20 km), B-DECIGO, LIGO in Livingston, and VIRGO, together with the effective strain amplitude of GW190725. The dimensionless characteristic strain is defined as  $\sqrt{f S_n}$  for the GW detectors and  $2f|h(f)|$  for the GW source.

### D. Fisher information matrix

We use the Fisher information matrix (FIM) [166] to simulate the GW source parameters' measurement errors. For a GW detector network with  $N$  interferometers, the FIM is given by

$$F_{ij} = \sum_{k=1}^N \left( \frac{\partial \tilde{h}_k(f)}{\partial \theta_i} \middle| \frac{\partial \tilde{h}_k(f)}{\partial \theta_j} \right), \quad (13)$$

where  $\theta_i$  denotes the  $i$ th parameter among the nine GW source parameters describing the GW signal, which are  $d_L, t_c, \mathcal{M}_c, \eta, \theta, \phi, \psi, \iota, \psi_c$ . Among them,  $\theta$  and  $\phi$  represent the colatitude and the longitude of the GW event, respectively.  $\psi$  is the polarization angle,  $\psi_c$  is the phase of GW when observed and  $t_c$  is the coalescence time.

The  $9 \times 9$  covariance matrix ( $Cov$ ) of the nine GW source parameters equal to the inverse of the FIM, and the measurement error of the  $i$ th GW parameter is given by  $\Delta \theta_i = \sqrt{Cov_{ii}}$ .

The sky localization error is given as

$$\Delta \Omega = 2\pi |\sin \theta| \sqrt{(\Delta \theta)^2 (\Delta \phi)^2 - (\Delta \theta \Delta \phi)^2}. \quad (14)$$

The total error of  $d_L$  is expressed as

$$\Delta d_L = \sqrt{(\Delta d_L^{\text{inst}})^2 + (\Delta d_L^{\text{lens}})^2 + (\Delta d_L^{\text{pv}})^2}, \quad (15)$$

where  $\Delta d_L^{\text{inst}}$  represents the instrumental error of  $d_L$ , estimated using FIM;  $\Delta d_L^{\text{lens}}$  denotes the weak-lensing error, given by [167, 168]

$$\Delta d_L^{\text{lens}}(z) = d_L \times 0.066 \left[ \frac{1 - (1+z)^{-0.25}}{0.25} \right]^{1.8}. \quad (16)$$

$\Delta d_L^{\text{pv}}(z)$  is the peculiar-velocity error, given by [169]

$$\Delta d_L^{\text{pv}}(z) = d_L \times \left[ 1 + \frac{c(1+z)^2}{H(z)d_L(z)} \right] \frac{\sqrt{\langle v^2 \rangle}}{c}, \quad (17)$$

where  $\sqrt{\langle v^2 \rangle}$  is the peculiar velocity of the GW source, set to  $\sqrt{\langle v^2 \rangle} = 500 \text{ km s}^{-1}$  [55].

### E. Identifying GW events' potential host galaxies

We rely on the three-dimensional (3D) localization capability of the GW detector to identify the potential host galaxies of GW sources. In our analysis, we model the 3D localization region of each GW event as a truncated cone, characterized by a radial range of  $[d_L^{\text{min}}, d_L^{\text{max}}] = [\bar{d}_L - 3\Delta d_L, \bar{d}_L + 3\Delta d_L]$  and an angular region defined by  $\chi^2 \leq 9.21$ . Here,  $\bar{d}_L$  represents the luminosity distance of the GW event,  $\Delta d_L$  denotes the  $1\sigma$  error of the luminosity distance measurement, obtained by Eq. (15), and  $\chi^2$  is expressed as

$$\chi^2 = (\theta - \bar{\theta}, \phi - \bar{\phi}) Cov'^{-1} \begin{pmatrix} \theta - \bar{\theta} \\ \phi - \bar{\phi} \end{pmatrix}, \quad (18)$$

where  $Cov'^{-1}$  is the  $2 \times 2$  covariance matrix of  $\theta$  and  $\phi$ . We obtain  $Cov'^{-1}$  by removing the rows and columns associated with the other parameters from the original  $9 \times 9$  covariance matrix estimated through the FIM analysis. The  $\chi^2$  value quantifies the deviation of a data point at  $(\theta, \phi)$  from the expected position at  $(\bar{\theta}, \bar{\phi})$  in terms of angle. The condition  $\chi^2 \leq 9.21$  corresponds to the 99% confidence region.

In order to match with the galaxy catalog, we convert the range of luminosity distances into a corresponding range of redshifts, denoted as  $[z_{\text{min}}, z_{\text{max}}]$ . Specifically,  $z^{\text{min}} = z(d_L^{\text{min}}, H_0^{\text{min}}, \Omega_m^{\text{min}})$  and  $z^{\text{max}} = z(d_L^{\text{max}}, H_0^{\text{max}}, \Omega_m^{\text{max}})$ , where  $H_0^{\text{min}}, H_0^{\text{max}}, \Omega_m^{\text{min}},$  and  $\Omega_m^{\text{max}}$  are the edge values of prior ranges of  $H_0$  and  $\Omega_m$ . Here, we set  $H_0 \in [60, 80] \text{ km s}^{-1} \text{ Mpc}^{-1}$  and  $\Omega_m \in [0.2, 0.4]$ . In summary, the potential host galaxies of each GW event are constrained within the range of  $[z_{\text{min}}, z_{\text{max}}]$  and  $\chi^2 \leq 9.21$ . It is worth noting that some GW events' localization ranges may be over the coverage of the galaxy catalog, also called the edge incompleteness [97]. We delete these events to avoid the system bias arising from them. Additionally, we calculate an angular localization weight for each potential host galaxy using the equation

$$w \propto \frac{1}{2\pi |Cov'|} \exp \left[ -\frac{1}{2} (\theta - \bar{\theta}, \phi - \bar{\phi}) Cov'^{-1} \begin{pmatrix} \theta - \bar{\theta} \\ \phi - \bar{\phi} \end{pmatrix} \right]. \quad (19)$$

### F. Cosmological parameter inferences

Inferring cosmological parameters using GW dark sirens requires the redshift information from galaxy catalogs. In this work, we generate a simplistic galaxy catalog by uniformly sampling galaxies within the comoving volume with a number density of  $0.02 \text{ Mpc}^{-3}$  (the median value of the result of Ref. [170]). Notably, the incompleteness of the galaxy catalog introduces a decline in the constraint precisions of cosmological parameters [95]. In our study, we adopt an optimistic assumption, assuming the galaxy catalog is complete up to  $z = 1$ , encompassing all host galaxies of GW events. Achieving such completeness may be facilitated by future survey missions such as Euclid [171], WFIRST [172], LSST [173, 174], and CSST [175–177]. For redshift uncertainties of galaxies in the mock galaxy catalog, we ignore the redshift measurement errors for galaxies at  $z \leq 0.1$  assuming these galaxies could be covered by future spectroscopic surveys [104, 178], and beyond this range, we mock the redshift uncertainties of galaxies as  $\Delta z(z) = 0.02(1+z)$ , which is the redshift measurement accuracy could be achieved by future photometric surveys [175].

We employ the Bayesian analysis to infer cosmological parameters  $\Omega$ . The posterior distribution of  $\Omega$  is given by

$$p(\Omega | \{D_{\text{GW}}\}) \propto p(\{D_{\text{GW}}\} | \Omega) p(\Omega), \quad (20)$$



where  $\{D_{\text{GW}}\}$  represents the GW dataset;  $p(\mathbf{\Omega})$  is the uniform prior distribution of  $\mathbf{\Omega}$ ; and  $p(\{D_{\text{GW}}\}|\mathbf{\Omega})$  signifies the likelihood function. As the observations are independent, the likelihood function can be expanded as the product of individual GW event likelihoods:

$$p(\{D_{\text{GW}}\}|\mathbf{\Omega}) = \prod_{i=1}^{N_{\text{GW}}} p(D_{\text{GW},i}|\mathbf{\Omega}), \quad (21)$$

where  $N_{\text{GW}}$  is the number of GW events. The likelihood function of a single GW event is given by

$$p(D_{\text{GW}}|\mathbf{\Omega}) = \frac{1}{\beta(\mathbf{\Omega})} \int p(D_{\text{GW}}|d_{\text{L}}(z, \mathbf{\Omega}))p(z)dz, \quad (22)$$

where  $p(D_{\text{GW}}|d_{\text{L}}(z, \mathbf{\Omega}))$  is the posterior distribution of the GW event's  $d_{\text{L}}$ , given by

$$p(D_{\text{GW}}|d_{\text{L}}(z, \mathbf{\Omega})) = \frac{1}{\sqrt{2\pi}\Delta d_{\text{L}}} \exp\left[-\frac{(\hat{d}_{\text{L}} - d_{\text{L}}(z, \mathbf{\Omega}))^2}{2\Delta d_{\text{L}}^2}\right], \quad (23)$$

where  $\Delta d_{\text{L}}$  is the 1- $\sigma$  error of  $d_{\text{L}}$  calculated using Eq. (15),  $\hat{d}_{\text{L}}$  is the luminosity distance of the GW event, and  $d_{\text{L}}(z, \mathbf{\Omega})$  is the theoretic luminosity distance calculated using Eq. (1) with  $z$  and  $\mathbf{\Omega}$ .  $p(z)$  is the prior distribution of the GW source's redshift  $z$  and is given by

$$p(z) = \frac{1}{N_{\text{in}}} \sum_{j=1}^{N_{\text{in}}} w_j \frac{1}{\sqrt{2\pi}\Delta z(\hat{z}_j)} \exp\left[-\frac{(\hat{z}_j - z)^2}{2(\Delta z(\hat{z}_j))^2}\right] \times \frac{dV_{\text{c}}}{dz}, \quad (24)$$

where  $\Delta(\hat{z}_j)$  is the redshift uncertainties of the  $j$ th potential host galaxy,  $w_j$  is the angular weight of the  $j$ th potential host galaxy calculated using Eq. (19), and  $V_{\text{c}}$  is the comoving volume.

The GW selection effect  $\beta(\mathbf{\Omega})$ , as delineated in Ref. [90], is considered, expressed as:

$$\beta(\mathbf{\Omega}) = \int p_{\text{det}}^{\text{GW}}(d_{\text{L}}(z, \mathbf{\Omega}))p(z)dz, \quad (25)$$

where  $p_{\text{det}}^{\text{GW}}(d_{\text{L}}(z, \mathbf{\Omega}))$  represents the detection probability of the GW event at  $d_{\text{L}}(z, \mathbf{\Omega})$ , which can be evaluated using Monte-Carlo integration, as explicated in Ref. [95],

$$p_{\text{det}}^{\text{GW}}(d_{\text{L}}) = \frac{1}{N_{\text{samp}}} \sum_{n=1}^{N_{\text{samp}}} p_{\text{det}}^{\text{GW}}(d_{\text{L}}|\boldsymbol{\theta}_n), \quad (26)$$

with

$$p_{\text{det}}^{\text{GW}}(d_{\text{L}}|\boldsymbol{\theta}_n) \approx \begin{cases} 1, & \text{if } \rho_n > \rho_{\text{th}}, \\ 0, & \text{otherwise,} \end{cases} \quad (27)$$

where  $N_{\text{samp}}$  is the number of samples, which is set to 50000, and  $\boldsymbol{\theta}_n$  is the GW source parameters other than  $d_{\text{L}}$  in the  $n$ th sampling.

### III. RESULTS AND DISCUSSION

In this section, we show the results of our analysis, including localization errors of GW events and constraints on cosmological parameters, and make relevant discussions.

Fig. 2 depicts the scatter distributions and cumulative distribution functions (CDFs) of  $\Delta d_{\text{L}}$ ,  $\Delta\Omega$ , and  $N_{\text{in}}$ . In panels (a) and (d), it's evident that  $\Delta d_{\text{L}}$  values of B-DECIGO and ET2CE are smaller than those of LVK for a half and one order of magnitude, respectively. This observation aligns with the sensitivity curves illustrated in Fig. 1, where B-DECIGO and ET2CE exhibit characteristic strains lower than LVK by approximately one and two orders of magnitude, respectively. Surprisingly, the improvement in measuring  $d_{\text{L}}$  with B-DECIGO-ET2CE compared to ET2CE alone is only slight. This is attributed to the  $\Delta d_{\text{L}}^{\text{inst}}$  values for ET2CE and B-DECIGO-ET2CE being very small at  $z < 1$ , and  $\Delta d_{\text{L}}$  is dominated by peculiar velocity errors and weak-lensing errors. In panels (b) and (e), the  $\Delta\Omega$  values for ET2CE and B-DECIGO are two orders of magnitude smaller than those for LVK, with B-DECIGO-ET2CE showing a one-order-of-magnitude improvement over B-DECIGO and ET2CE. The scatter distribution of  $N_{\text{in}}$  shown in panel (c) reveals that for  $d_{\text{L}} < 1000$  Mpc, the  $N_{\text{in}}$  values of GW events identified by ET2CE and B-DECIGO is approximately one order of magnitude smaller than that by LVK, consistent with our analysis of localization errors. However, at larger  $d_{\text{L}}$  values, the  $N_{\text{in}}$  distribution of LVK overlaps with or even lower than those of ET2CE and B-DECIGO. This discrepancy is primarily attributed to the GLADE+ catalog used by LVK, which exhibits decreasing completeness with increasing  $d_{\text{L}}$ , dropping to 20% at  $d_{\text{L}} = 800$  Mpc.

Table I presents the situation of GW events used in analysis and summarizes the results of cosmological constraints. In the first row, we show the number of GW events used in cosmological inference for each GW detector scenario. In analysis, we artificially select well-localized GW events with  $N_{\text{in}} < 10000$ . Poorly localized GW events cannot provide efficient cosmological parameter inference (the posterior distributions of parameters are very flat), and removing them has little impact on the final parameter error estimation and can also reduce the computation costs. In addition, as is mentioned in Sec. II E, we exclude GW events influenced by the edge incompleteness. In the second row, we show the number of GW events with  $N_{\text{in}} = 1$ . GW events with  $N_{\text{in}} = 1$  are efficient bright sirens, with redshifts determined by the follow-up spectroscopic observation. We find that using the multi-band GW synergetic detection can significantly increase the number of GW events that are well localized and can be used in cosmological parameter inference, and the number of  $N_{\text{in}} = 1$  events is improved by 3–24 times. In the third to sixth rows, we report parameter constraints in the  $\Lambda$ CDM model and make further discussions in the following paragraphs.

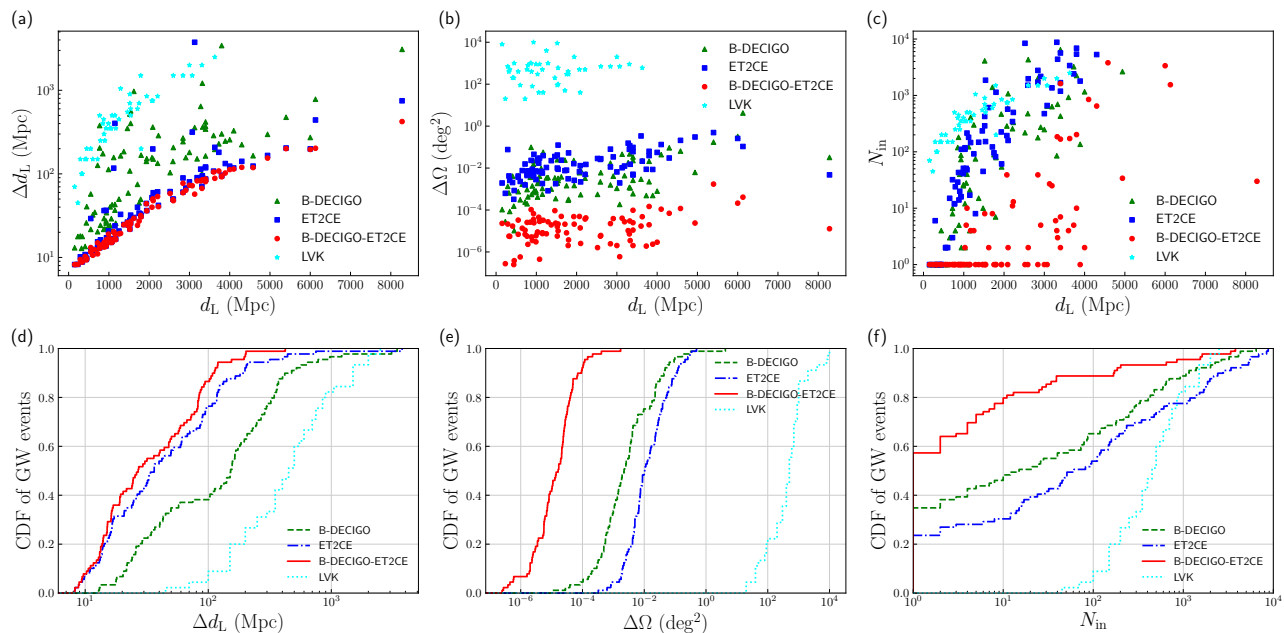


FIG. 2: The localization error and the number of potential host galaxies of GW events. Panel (a): The results of  $\Delta d_L$  across four GW detector configurations: ET2CE network, B-DECIGO, B-DECIGO-ET2CE network, and LVK network. Panel (b): Similar to the panel (a), but showcasing the results for  $\Delta\Omega$ . Panel (c): Similar to panel (a), but showcasing the number of potential host galaxies  $N_{\text{in}}$  of each GW event. Panels (d)–(f): The cumulative distribution functions (CDF) of GW events on  $\Delta d_L$ ,  $\Delta\Omega$ , and  $N_{\text{in}}$ , respectively.

In Fig. 3, we present the constraint results of B-DECIGO, ET2CE, and B-DECIGO-ET2CE in the  $H_0$ – $\Omega$  plane. They depict the optimal situations of the space-based and ground-based detectors and the multi-band GW synergetic detector network, respectively. Using the multi-band GW synergetic detection, B-DECIGO-ET2CE outperforms ET2CE and B-DECIGO, exhibiting enhanced constraint precisions on  $H_0$  by 69.2% and 73.3%, and on  $\Omega_m$  by 85.1% and 78.6%, respectively. Despite B-DECIGO-ET2CE shares a similar  $\Delta d_L$  distribution with ET2CE, as seen in panels (a) and (d) of Fig. 2, its lower  $\Delta\Omega$  leads to the smaller  $N_{\text{in}}$ , indicating more precise redshift inference than ET2CE, which enhance precision in cosmological parameter constraints through the distance-redshift relation. Compared with B-DECIGO, as shown in Fig. 2, B-DECIGO-ET2CE has advantages in both  $\Delta d_L$  and  $N_{\text{in}}$ .

In Fig 4, we present the  $H_0$  constraint precisions of all GW detector scenarios. 2CE possesses an extremely marginal enhancement over ET, and when considering precision to two decimal places, both exhibit the constraint precision on  $H_0$  of 2.60%. The enhancement of B-DECIGO compared with 2CE is significant, with a  $H_0$  constraint precision enhancement of 30.8%. When using the multi-band GW synergetic detection, the precision constraint precisions of  $H_0$  are below 0.6%, better than the Planck 2018 CMB+BAO result [7]. Even in the worst case of using multi-band GW synergetic detection, B-DECIGO-ET significantly outperforms the best case of not using (ET2CE), with the  $H_0$  constraint pre-

cision improved by 64.7%. Notably, with an increasing number of ground-based GW detectors in the multi-band GW synergetic detector network, there are only slight improvements in  $H_0$  constraint precisions. Specifically, B-DECIGO-2CE is 5.5% better than B-DECIGO-ET, and B-DECIGO-ET2CE exhibits a 7.7% improvement over B-DECIGO-2CE. A similar situation also appears in constraining  $\Omega_m$ , as shown in Table I. The  $\Omega_m$  constraint precision of B-DECIGO-ET is improved by 74.9% compared with that of B-DECIGO. Meanwhile, B-DECIGO-2CE is slightly better than B-DECIGO-ET by 2.5%, and B-DECIGO-ET2CE is 12.4% better than B-DECIGO-2CE. Our results indicate that the multi-band GW synergetic observation can significantly enhance constraint precisions of cosmological parameters and may help resolve the Hubble tension.

Compared with the latest reality dark siren analysis in Ref. [101], our constraint precisions on  $H_0$  show a remarkable improvement of at least 97.5%. This improvement is due to several factors. Firstly, we incorporate anticipated advancements in 3G ground-based GW detectors and B-DECIGO, which are expected to be far more sensitive than current detectors. Secondly, our adoption of a multi-band GW synergetic detection strategy significantly enhances SNRs and localization precisions, leading to a greater number of usable GW events. Lastly, we optimistically assume a complete galaxy catalog up to  $z \leq 1$ , as discussed in Sec. III F.

TABLE I: The number of GW events used in cosmological inference  $N_{\text{GW}}$  and the number of GW events with  $N_{\text{in}} = 1$ , alongside the absolute errors ( $1\sigma$ ) and the relative errors of the cosmological parameters in the  $\Lambda\text{CDM}$  model. Here the unit of  $H_0$  is  $\text{km s}^{-1} \text{Mpc}^{-1}$ .

Result type	ET	2CE	B-DECIGO	ET2CE	B-DECIGO-ET	B-DECIGO-2CE	B-DECIGO-ET2CE
$N_{\text{GW}}$	37	51	68	75	87	87	88
$N_{\text{in}} = 1$	2	2	10	7	40	45	50
$\sigma(\Omega_{\text{m}})$	–	–	0.135	0.180	0.027	0.026	0.023
$\sigma(H_0)$	1.70	1.70	1.20	1.05	0.37	0.35	0.32
$\varepsilon(\Omega_{\text{m}})$	–	–	33.75%	48.60%	8.46%	8.25%	7.23%
$\varepsilon(H_0)$	2.60%	2.60%	1.80%	1.56%	0.55%	0.52%	0.48%

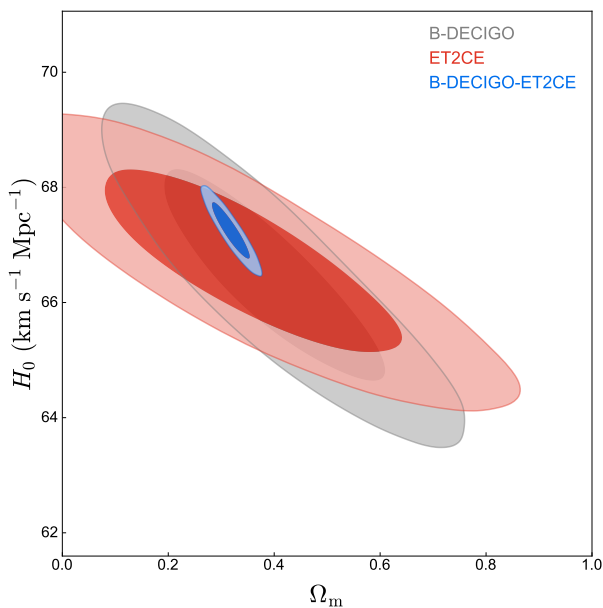


FIG. 3: Two-dimensional marginalized contours (68.3% and 95.4% confidence level) in the  $\Omega_{\text{m}}-H_0$  plane by using B-DECIGO, ET2CE and B-DECIGO-ET2CE mock data for the  $\Lambda\text{CDM}$  model.

#### IV. CONCLUSION

GW standard sirens have significant potential as a cosmological probe for measuring absolute distances and can constrain the cosmic expansion history through the distance-redshift relation. The statistical galaxy catalog method provides redshifts for dark sirens without electromagnetic counterparts, relying on GW localization precisions. Multi-band GW synergetic detection can improve SNRs and localization precisions. In this paper, we explore how the multi-band GW synergetic detection of B-DECIGO and 3G ground-based GW detectors enhances dark siren cosmology.

Firstly, we simulate GW signals using the IMRPhe-

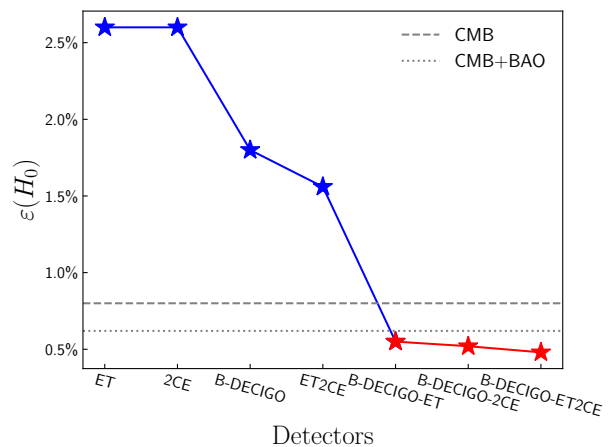


FIG. 4: The relative errors of  $H_0$  by using ET, 2CE, B-DECIGO, ET2CE, B-DECIGO-ET, B-DECIGO-2CE, and B-DECIGO-ET2CE mock data. The gray horizontal dashed and point lines represent the constraint precisions of Planck2018 CMB and CMB+BAO data.

nomA waveform model with GW source parameters set to the best-fit values of the parameter posteriors of 89 events in GWTC-3. Secondly, we use the Fisher information matrix to estimate the localization precisions of B-DECIGO, ET, CE, and the GW detector networks composed of them. Thirdly, we identify potential host galaxies of dark sirens by cross-matching the GW localization region with a mock galaxy catalog complete up to  $z = 1$ . Finally, we use Bayesian analysis to infer cosmological parameters in the  $\Lambda\text{CDM}$  model.

Our results show that with only 89 GW events in GWTC-3, the multi-band GW synergetic observation of B-DECIGO and 3G ground-based GW detectors can constrain  $H_0$  to around 0.5%, showing significant potential in dark siren cosmology. In comparison, without the multi-band synergetic observation strategy, B-DECIGO and 3G ground-based GW detectors can only constrain  $H_0$  to 1.5%–2.6%. Using the multi-band synergetic de-

tection strategy has more than 67% improvement in the constraint precision on  $H_0$  compared with not using it.

We find that multi-band GW synergetic observation enhances dark siren cosmology in the following aspects: (1) Extending the detection frequency range to improve the SNR, helping us to include more GW events in the dark siren analysis. (2) Enhancing the GW localization precisions, reducing the number of potential host galaxies and helping to infer the redshifts of dark sirens. (3) Increasing the number of dark sirens with  $N_{\text{in}} = 1$ , which are de facto bright sirens. We conclude that the multi-band GW synergetic observation has a significant poten-

tial enhancement to dark siren cosmology.

### Acknowledgements

This work was supported by the National SKA Program of China (Grants Nos. 2022SKA0110200 and 2022SKA0110203), the National Natural Science Foundation of China (Grants Nos. 11975072, 11875102, and 11835009), the National 111 Project (Grant No. B16009), and the China Scholarship Council.

- 
- [1] L. Verde, T. Treu, and A. G. Riess, *Nature Astron.* **3**, 891 (2019), arXiv:1907.10625 [astro-ph.CO] .
- [2] A. G. Riess, *Nature Rev. Phys.* **2**, 10 (2019), arXiv:2001.03624 [astro-ph.CO] .
- [3] E. Di Valentino, O. Mena, S. Pan, L. Visinelli, W. Yang, A. Melchiorri, D. F. Mota, A. G. Riess, and J. Silk, *Class. Quant. Grav.* **38**, 153001 (2021), arXiv:2103.01183 [astro-ph.CO] .
- [4] E. Abdalla *et al.*, *JHEAp* **34**, 49 (2022), arXiv:2203.06142 [astro-ph.CO] .
- [5] M. Kamionkowski and A. G. Riess, (2022), arXiv:2211.04492 [astro-ph.CO] .
- [6] L. Perivolaropoulos and F. Skara, *New Astron. Rev.* **95**, 101659 (2022), arXiv:2105.05208 [astro-ph.CO] .
- [7] N. Aghanim *et al.* (Planck), *Astron. Astrophys.* **641**, A6 (2020), [Erratum: *Astron. Astrophys.* 652, C4 (2021)], arXiv:1807.06209 [astro-ph.CO] .
- [8] A. G. Riess *et al.*, *Astrophys. J. Lett.* **934**, L7 (2022), arXiv:2112.04510 [astro-ph.CO] .
- [9] M. Li, X.-D. Li, Y.-Z. Ma, X. Zhang, and Z. Zhang, *JCAP* **09**, 021 (2013), arXiv:1305.5302 [astro-ph.CO] .
- [10] V. Poulin, T. L. Smith, T. Karwal, and M. Kamionkowski, *Phys. Rev. Lett.* **122**, 221301 (2019), arXiv:1811.04083 [astro-ph.CO] .
- [11] J.-F. Zhang, Y.-H. Li, and X. Zhang, *Phys. Lett. B* **740**, 359 (2015), arXiv:1403.7028 [astro-ph.CO] .
- [12] J.-F. Zhang, Y.-H. Li, and X. Zhang, *Eur. Phys. J. C* **74**, 2954 (2014), arXiv:1404.3598 [astro-ph.CO] .
- [13] M.-M. Zhao, D.-Z. He, J.-F. Zhang, and X. Zhang, *Phys. Rev. D* **96**, 043520 (2017), arXiv:1703.08456 [astro-ph.CO] .
- [14] L. Feng, J.-F. Zhang, and X. Zhang, *Eur. Phys. J. C* **77**, 418 (2017), arXiv:1703.04884 [astro-ph.CO] .
- [15] M. Li, X. Li, and X. Zhang, *Sci. China Phys. Mech. Astron.* **53**, 1631 (2010), arXiv:0912.3988 [astro-ph.CO] .
- [16] J.-F. Zhang, J.-J. Geng, and X. Zhang, *JCAP* **10**, 044 (2014), arXiv:1408.0481 [astro-ph.CO] .
- [17] R.-Y. Guo, J.-F. Zhang, and X. Zhang, *JCAP* **02**, 054 (2019), arXiv:1809.02340 [astro-ph.CO] .
- [18] L.-Y. Gao, Z.-W. Zhao, S.-S. Xue, and X. Zhang, *JCAP* **07**, 005 (2021), arXiv:2101.10714 [astro-ph.CO] .
- [19] R.-G. Cai, Z.-K. Guo, L. Li, S.-J. Wang, and W.-W. Yu, *Phys. Rev. D* **103**, 121302 (2021), arXiv:2102.02020 [astro-ph.CO] .
- [20] W. Yang, S. Pan, E. Di Valentino, R. C. Nunes, S. Vagnozzi, and D. F. Mota, *JCAP* **09**, 019 (2018), arXiv:1805.08252 [astro-ph.CO] .
- [21] E. Di Valentino *et al.*, *Astropart. Phys.* **131**, 102605 (2021), arXiv:2008.11284 [astro-ph.CO] .
- [22] E. Di Valentino, A. Melchiorri, O. Mena, and S. Vagnozzi, *Phys. Dark Univ.* **30**, 100666 (2020), arXiv:1908.04281 [astro-ph.CO] .
- [23] E. Di Valentino, A. Melchiorri, O. Mena, and S. Vagnozzi, *Phys. Rev. D* **101**, 063502 (2020), arXiv:1910.09853 [astro-ph.CO] .
- [24] M. Liu, Z. Huang, X. Luo, H. Miao, N. K. Singh, and L. Huang, *Sci. China Phys. Mech. Astron.* **63**, 290405 (2020), arXiv:1912.00190 [astro-ph.CO] .
- [25] X. Zhang and Q.-G. Huang, *Sci. China Phys. Mech. Astron.* **63**, 290402 (2020), arXiv:1911.09439 [astro-ph.CO] .
- [26] Q. Ding, T. Nakama, and Y. Wang, *Sci. China Phys. Mech. Astron.* **63**, 290403 (2020), arXiv:1912.12600 [astro-ph.CO] .
- [27] H. Li and X. Zhang, *Sci. Bull.* **65**, 1419 (2020), arXiv:2005.10458 [astro-ph.CO] .
- [28] L.-F. Wang, J.-H. Zhang, D.-Z. He, J.-F. Zhang, and X. Zhang, *Mon. Not. Roy. Astron. Soc.* **514**, 1433 (2022), arXiv:2102.09331 [astro-ph.CO] .
- [29] S. Vagnozzi, F. Pacucci, and A. Loeb, *JHEAp* **36**, 27 (2022), arXiv:2105.10421 [astro-ph.CO] .
- [30] S. Vagnozzi, *Phys. Rev. D* **104**, 063524 (2021), arXiv:2105.10425 [astro-ph.CO] .
- [31] S. Vagnozzi, *Phys. Rev. D* **102**, 023518 (2020), arXiv:1907.07569 [astro-ph.CO] .
- [32] R.-Y. Guo, J.-F. Zhang, and X. Zhang, *Sci. China Phys. Mech. Astron.* **63**, 290406 (2020), arXiv:1910.13944 [astro-ph.CO] .
- [33] L. Feng, D.-Z. He, H.-L. Li, J.-F. Zhang, and X. Zhang, *Sci. China Phys. Mech. Astron.* **63**, 290404 (2020), arXiv:1910.03872 [astro-ph.CO] .
- [34] M.-X. Lin, W. Hu, and M. Raveri, *Phys. Rev. D* **102**, 123523 (2020), arXiv:2009.08974 [astro-ph.CO] .
- [35] L.-Y. Gao, S.-S. Xue, and X. Zhang, (2022), arXiv:2212.13146 [astro-ph.CO] .
- [36] Z.-W. Zhao, J.-G. Zhang, Y. Li, J.-M. Zou, J.-F. Zhang, and X. Zhang, (2022), arXiv:2212.13433 [astro-ph.CO] .
- [37] N. Dalal, D. E. Holz, S. A. Hughes, and B. Jain, *Phys. Rev. D* **74**, 063006 (2006), arXiv:astro-ph/0601275 .
- [38] C. Cutler and D. E. Holz, *Phys. Rev. D* **80**, 104009



- (2009), arXiv:0906.3752 [astro-ph.CO] .
- [39] S. Nissanke, D. E. Holz, S. A. Hughes, N. Dalal, and J. L. Sievers, *Astrophys. J.* **725**, 496 (2010), arXiv:0904.1017 [astro-ph.CO] .
- [40] W. Zhao, C. Van Den Broeck, D. Baskaran, and T. G. F. Li, *Phys. Rev. D* **83**, 023005 (2011), arXiv:1009.0206 [astro-ph.CO] .
- [41] R.-G. Cai and T. Yang, *Phys. Rev. D* **95**, 044024 (2017), arXiv:1608.08008 [astro-ph.CO] .
- [42] R.-G. Cai, Z. Cao, Z.-K. Guo, S.-J. Wang, and T. Yang, *Natl. Sci. Rev.* **4**, 687 (2017), arXiv:1703.00187 [gr-qc] .
- [43] R.-G. Cai, T.-B. Liu, X.-W. Liu, S.-J. Wang, and T. Yang, *Phys. Rev. D* **97**, 103005 (2018), arXiv:1712.00952 [astro-ph.CO] .
- [44] R.-G. Cai and T. Yang, *EPJ Web Conf.* **168**, 01008 (2018), arXiv:1709.00837 [astro-ph.CO] .
- [45] X.-N. Zhang, L.-F. Wang, J.-F. Zhang, and X. Zhang, *Phys. Rev. D* **99**, 063510 (2019), arXiv:1804.08379 [astro-ph.CO] .
- [46] M. Du, W. Yang, L. Xu, S. Pan, and D. F. Mota, *Phys. Rev. D* **100**, 043535 (2019), arXiv:1812.01440 [astro-ph.CO] .
- [47] X. Zhang, *Sci. China Phys. Mech. Astron.* **62**, 110431 (2019), arXiv:1905.11122 [astro-ph.CO] .
- [48] E. Belgacem, Y. Dirian, S. Foffa, E. J. Howell, M. Maggiore, and T. Regimbau, *JCAP* **08**, 015 (2019), arXiv:1907.01487 [astro-ph.CO] .
- [49] M. Safarzadeh, E. Berger, K. K. Y. Ng, H.-Y. Chen, S. Vitale, C. Whittle, and E. Scannapieco, *Astrophys. J. Lett.* **878**, L13 (2019), arXiv:1904.10976 [astro-ph.HE] .
- [50] J.-F. Zhang, H.-Y. Dong, J.-Z. Qi, and X. Zhang, *Eur. Phys. J. C* **80**, 217 (2020), arXiv:1906.07504 [astro-ph.CO] .
- [51] J.-F. Zhang, M. Zhang, S.-J. Jin, J.-Z. Qi, and X. Zhang, *JCAP* **09**, 068 (2019), arXiv:1907.03238 [astro-ph.CO] .
- [52] W. Yang, S. Pan, E. Di Valentino, B. Wang, and A. Wang, *JCAP* **05**, 050 (2020), arXiv:1904.11980 [astro-ph.CO] .
- [53] R. R. A. Bacheaga, A. A. Costa, E. Abdalla, and K. S. F. Fornazier, *JCAP* **05**, 021 (2020), arXiv:1906.08909 [astro-ph.CO] .
- [54] Z. Chang, Q.-G. Huang, S. Wang, and Z.-C. Zhao, *Eur. Phys. J. C* **79**, 177 (2019).
- [55] J.-h. He, *Phys. Rev. D* **100**, 023527 (2019), arXiv:1903.11254 [astro-ph.CO] .
- [56] Z.-W. Zhao, L.-F. Wang, J.-F. Zhang, and X. Zhang, *Sci. Bull.* **65**, 1340 (2020), arXiv:1912.11629 [astro-ph.CO] .
- [57] L.-F. Wang, Z.-W. Zhao, J.-F. Zhang, and X. Zhang, *JCAP* **11**, 012 (2020), arXiv:1907.01838 [astro-ph.CO] .
- [58] H.-Y. Chen, *Phys. Rev. Lett.* **125**, 201301 (2020), arXiv:2006.02779 [astro-ph.HE] .
- [59] H.-Y. Chen, P. S. Cowperthwaite, B. D. Metzger, and E. Berger, *Astrophys. J. Lett.* **908**, L4 (2021), arXiv:2011.01211 [astro-ph.CO] .
- [60] S.-J. Jin, D.-Z. He, Y. Xu, J.-F. Zhang, and X. Zhang, *JCAP* **03**, 051 (2020), arXiv:2001.05393 [astro-ph.CO] .
- [61] A. Mitra, J. Mifsud, D. F. Mota, and D. Parkinson, *Mon. Not. Roy. Astron. Soc.* **502**, 5563 (2021), arXiv:2010.00189 [astro-ph.CO] .
- [62] S. Borhanian, A. Dhani, A. Gupta, K. G. Arun, and B. S. Sathyaprakash, *Astrophys. J. Lett.* **905**, L28 (2020), arXiv:2007.02883 [astro-ph.CO] .
- [63] N. B. Hogg, M. Martinelli, and S. Nesseris, *JCAP* **12**, 019 (2020), arXiv:2007.14335 [astro-ph.CO] .
- [64] R. C. Nunes, *Phys. Rev. D* **102**, 024071 (2020), arXiv:2007.07750 [gr-qc] .
- [65] J.-Z. Qi, S.-J. Jin, X.-L. Fan, J.-F. Zhang, and X. Zhang, *JCAP* **12**, 042 (2021), arXiv:2102.01292 [astro-ph.CO] .
- [66] M.-D. Cao, J. Zheng, J.-Z. Qi, X. Zhang, and Z.-H. Zhu, *Astrophys. J.* **934**, 108 (2022), arXiv:2112.14564 [astro-ph.CO] .
- [67] X. Fu, L. Zhou, J. Yang, Z.-Y. Lu, Y. Yang, and G. Tang, *Chin. Phys. C* **45**, 065104 (2021).
- [68] L. Bian *et al.*, *Sci. China Phys. Mech. Astron.* **64**, 120401 (2021), arXiv:2106.10235 [gr-qc] .
- [69] C. Ye and M. Fishbach, *Phys. Rev. D* **104**, 043507 (2021), arXiv:2103.14038 [astro-ph.CO] .
- [70] S.-J. Jin, L.-F. Wang, P.-J. Wu, J.-F. Zhang, and X. Zhang, *Phys. Rev. D* **104**, 103507 (2021), arXiv:2106.01859 [astro-ph.CO] .
- [71] J. M. S. de Souza, R. Sturani, and J. Alcaniz, *JCAP* **03**, 025 (2022), arXiv:2110.13316 [gr-qc] .
- [72] J. Yu, H. Song, S. Ai, H. Gao, F. Wang, Y. Wang, Y. Lu, W. Fang, and W. Zhao, *Astrophys. J.* **916**, 54 (2021), arXiv:2104.12374 [astro-ph.HE] .
- [73] T. Zhu, W. Zhao, and A. Wang, (2022), arXiv:2210.05259 [gr-qc] .
- [74] P.-J. Wu, Y. Shao, S.-J. Jin, and X. Zhang, *JCAP* **06**, 052 (2023), arXiv:2202.09726 [astro-ph.CO] .
- [75] S.-J. Jin, R.-Q. Zhu, L.-F. Wang, H.-L. Li, J.-F. Zhang, and X. Zhang, *Commun. Theor. Phys.* **74**, 105404 (2022), arXiv:2204.04689 [astro-ph.CO] .
- [76] W.-T. Hou, J.-Z. Qi, T. Han, J.-F. Zhang, S. Cao, and X. Zhang, *JCAP* **05**, 017 (2023), arXiv:2211.10087 [astro-ph.CO] .
- [77] M. Califano, I. de Martino, D. Vernieri, and S. Capozziello, *Phys. Rev. D* **107**, 123519 (2023), arXiv:2208.13999 [astro-ph.CO] .
- [78] L.-F. Wang, Y. Shao, G.-P. Zhang, J.-F. Zhang, and X. Zhang, (2022), arXiv:2201.00607 [astro-ph.CO] .
- [79] A. Dhani, S. Borhanian, A. Gupta, and B. Sathyaprakash, (2022), arXiv:2212.13183 [gr-qc] .
- [80] E. O. Colgáin, in *17th Italian-Korean Symposium on Relativistic Astrophysics* (2022) arXiv:2203.03956 [astro-ph.CO] .
- [81] S.-J. Jin, T.-N. Li, J.-F. Zhang, and X. Zhang, *JCAP* **08**, 070 (2023), arXiv:2202.11882 [gr-qc] .
- [82] S.-J. Jin, S.-S. Xing, Y. Shao, J.-F. Zhang, and X. Zhang, *Chin. Phys. C* **47**, 065104 (2023), arXiv:2301.06722 [astro-ph.CO] .
- [83] T. Han, S.-J. Jin, J.-F. Zhang, and X. Zhang, (2023), arXiv:2309.14965 [astro-ph.CO] .
- [84] T.-N. Li, S.-J. Jin, H.-L. Li, J.-F. Zhang, and X. Zhang, *Astrophys. J.* **963**, 52 (2024), arXiv:2310.15879 [astro-ph.CO] .
- [85] S.-J. Jin, R.-Q. Zhu, J.-Y. Song, T. Han, J.-F. Zhang, and X. Zhang, (2023), arXiv:2309.11900 [astro-ph.CO] .
- [86] Z. Guo, *Science China Physics, Mechanics & Astronomy* **65** (2021).
- [87] B. F. Schutz, *Nature* **323**, 310 (1986).
- [88] D. E. Holz and S. A. Hughes, *Astrophys. J.* **629**, 15 (2005), arXiv:astro-ph/0504616 .

- [89] W. Del Pozzo, *Phys. Rev. D* **86**, 043011 (2012), [arXiv:1108.1317 \[astro-ph.CO\]](#) .
- [90] H.-Y. Chen, M. Fishbach, and D. E. Holz, *Nature* **562**, 545 (2018), [arXiv:1712.06531 \[astro-ph.CO\]](#) .
- [91] M. Fishbach *et al.* (LIGO Scientific, Virgo), *Astrophys. J. Lett.* **871**, L13 (2019), [arXiv:1807.05667 \[astro-ph.CO\]](#) .
- [92] R. Nair, S. Bose, and T. D. Saini, *Phys. Rev. D* **98**, 023502 (2018), [arXiv:1804.06085 \[astro-ph.CO\]](#) .
- [93] M. Soares-Santos *et al.* (DES, LIGO Scientific, Virgo), *Astrophys. J. Lett.* **876**, L7 (2019), [arXiv:1901.01540 \[astro-ph.CO\]](#) .
- [94] B. P. Abbott *et al.* (LIGO Scientific, Virgo, VIRGO), *Astrophys. J.* **909**, 218 (2021), [arXiv:1908.06060 \[astro-ph.CO\]](#) .
- [95] R. Gray *et al.*, *Phys. Rev. D* **101**, 122001 (2020), [arXiv:1908.06050 \[gr-qc\]](#) .
- [96] A. Palmese *et al.* (DES), *Astrophys. J. Lett.* **900**, L33 (2020), [arXiv:2006.14961 \[astro-ph.CO\]](#) .
- [97] J. Yu, Y. Wang, W. Zhao, and Y. Lu, *Mon. Not. Roy. Astron. Soc.* **498**, 1786 (2020), [arXiv:2003.06586 \[astro-ph.CO\]](#) .
- [98] A. Finke, S. Foffa, F. Iacovelli, M. Maggiore, and M. Mancarella, *JCAP* **08**, 026 (2021), [arXiv:2101.12660 \[astro-ph.CO\]](#) .
- [99] H. Leandro, V. Marra, and R. Sturani, *Phys. Rev. D* **105**, 023523 (2022), [arXiv:2109.07537 \[gr-qc\]](#) .
- [100] A. Palmese, C. R. Bom, S. Mucesh, and W. G. Hartley, *Astrophys. J.* **943**, 56 (2023), [arXiv:2111.06445 \[astro-ph.CO\]](#) .
- [101] R. Abbott *et al.* (LIGO Scientific, Virgo, KAGRA), *Astrophys. J.* **949**, 76 (2023), [arXiv:2111.03604 \[astro-ph.CO\]](#) .
- [102] T. Yang, R.-G. Cai, and H. M. Lee, *JCAP* **10**, 061 (2022), [arXiv:2208.10998 \[gr-qc\]](#) .
- [103] J. R. Gair *et al.*, *Astron. J.* **166**, 22 (2023), [arXiv:2212.08694 \[gr-qc\]](#) .
- [104] J.-Y. Song, L.-F. Wang, Y. Li, Z.-W. Zhao, J.-F. Zhang, W. Zhao, and X. Zhang, (2022), [arXiv:2212.00531 \[astro-ph.CO\]](#) .
- [105] N. Muttoni, D. Laghi, N. Tamanini, S. Marsat, and D. Izquierdo-Villalba, *Phys. Rev. D* **108**, 043543 (2023), [arXiv:2303.10693 \[astro-ph.CO\]](#) .
- [106] B. P. Abbott *et al.* (LIGO Scientific, Virgo), *Phys. Rev. X* **9**, 031040 (2019), [arXiv:1811.12907 \[astro-ph.HE\]](#) .
- [107] R. Abbott *et al.* (LIGO Scientific, Virgo), *Phys. Rev. X* **11**, 021053 (2021), [arXiv:2010.14527 \[gr-qc\]](#) .
- [108] R. Abbott *et al.* (LIGO Scientific, VIRGO, KAGRA), (2021), [arXiv:2111.03606 \[gr-qc\]](#) .
- [109] B. P. Abbott *et al.* (LIGO Scientific, Virgo, 1M2H, Dark Energy Camera GW-E, DES, DLT40, Las Cumbres Observatory, VINROUGE, MASTER), *Nature* **551**, 85 (2017), [arXiv:1710.05835 \[astro-ph.CO\]](#) .
- [110] G. Dálya, G. Galgóczi, L. Dobos, Z. Frei, I. S. Heng, R. Macas, C. Messenger, P. Raffai, and R. S. de Souza, *Mon. Not. Roy. Astron. Soc.* **479**, 2374 (2018), [arXiv:1804.05709 \[astro-ph.HE\]](#) .
- [111] G. Dálya *et al.*, *Mon. Not. Roy. Astron. Soc.* **514**, 1403 (2022), [arXiv:2110.06184 \[astro-ph.CO\]](#) .
- [112] R. Abbott *et al.* (KAGRA, VIRGO, LIGO Scientific), *Phys. Rev. X* **13**, 041039 (2023), [arXiv:2111.03606 \[gr-qc\]](#) .
- [113] M. Punturo *et al.*, *Class. Quant. Grav.* **27**, 194002 (2010).
- [114] B. P. Abbott *et al.* (LIGO Scientific), *Class. Quant. Grav.* **34**, 044001 (2017), [arXiv:1607.08697 \[astro-ph.IM\]](#) .
- [115] P. Amaro-Seoane *et al.* (LISA), (2017), [arXiv:1702.00786 \[astro-ph.IM\]](#) .
- [116] T. Robson, N. J. Cornish, and C. Liu, *Class. Quant. Grav.* **36**, 105011 (2019), [arXiv:1803.01944 \[astro-ph.HE\]](#) .
- [117] P. Auclair *et al.* (LISA Cosmology Working Group), (2022), [arXiv:2204.05434 \[astro-ph.CO\]](#) .
- [118] W.-R. Hu and Y.-L. Wu, *Natl. Sci. Rev.* **4**, 685 (2017).
- [119] W.-H. Ruan, Z.-K. Guo, R.-G. Cai, and Y.-Z. Zhang, *Int. J. Mod. Phys. A* **35**, 2050075 (2020), [arXiv:1807.09495 \[gr-qc\]](#) .
- [120] Y.-L. Wu, *Int. J. Mod. Phys. A* **33**, 1844014 (2018), [arXiv:1805.10119 \[physics.gen-ph\]](#) .
- [121] J. Luo *et al.* (TianQin), *Class. Quant. Grav.* **33**, 035010 (2016), [arXiv:1512.02076 \[astro-ph.IM\]](#) .
- [122] H.-T. Wang *et al.*, *Phys. Rev. D* **100**, 043003 (2019), [arXiv:1902.04423 \[astro-ph.HE\]](#) .
- [123] S. Liu, Y.-M. Hu, J.-d. Zhang, and J. Mei, *Phys. Rev. D* **101**, 103027 (2020), [arXiv:2004.14242 \[astro-ph.HE\]](#) .
- [124] J. Luo *et al.*, *Class. Quant. Grav.* **37**, 185013 (2020), [arXiv:2008.09534 \[physics.ins-det\]](#) .
- [125] V. K. Milyukov, *Astron. Rep.* **64**, 1067 (2020).
- [126] J. Mei *et al.* (TianQin), *PTEP* **2021**, 05A107 (2021), [arXiv:2008.10332 \[gr-qc\]](#) .
- [127] A. Sesana, *Phys. Rev. Lett.* **116**, 231102 (2016), [arXiv:1602.06951 \[gr-qc\]](#) .
- [128] S. Vitale, *Phys. Rev. Lett.* **117**, 051102 (2016), [arXiv:1605.01037 \[gr-qc\]](#) .
- [129] S. Isoyama, H. Nakano, and T. Nakamura, *PTEP* **2018**, 073E01 (2018), [arXiv:1802.06977 \[gr-qc\]](#) .
- [130] D. Gerosa, S. Ma, K. W. K. Wong, E. Berti, R. O’Shaughnessy, Y. Chen, and K. Belczynski, *Phys. Rev. D* **99**, 103004 (2019), [arXiv:1902.00021 \[astro-ph.HE\]](#) .
- [131] Z. Carson and K. Yagi, *Phys. Rev. D* **101**, 044047 (2020), [arXiv:1911.05258 \[gr-qc\]](#) .
- [132] A. Sesana, *J. Phys. Conf. Ser.* **840**, 012018 (2017), [arXiv:1702.04356 \[astro-ph.HE\]](#) .
- [133] Y. Zhao, Y. Lu, C. Yan, Z. Chen, and W.-T. Ni, *Mon. Not. Roy. Astron. Soc.* **522**, 2951 (2023), [arXiv:2306.02636 \[astro-ph.HE\]](#) .
- [134] A. Klein *et al.*, (2022), [arXiv:2204.03423 \[astro-ph.HE\]](#) .
- [135] F. Zhang, X. Chen, L. Shao, and K. Inayoshi, *Astrophys. J.* **923**, 139 (2021), [arXiv:2109.14842 \[astro-ph.HE\]](#) .
- [136] N. Muttoni, A. Mangiagli, A. Sesana, D. Laghi, W. Del Pozzo, D. Izquierdo-Villalba, and M. Rosati, *Phys. Rev. D* **105**, 043509 (2022), [arXiv:2109.13934 \[astro-ph.CO\]](#) .
- [137] K. Jani, D. Shoemaker, and C. Cutler, *Nature Astron.* **4**, 260 (2019), [arXiv:1908.04985 \[gr-qc\]](#) .
- [138] C. Liu, L. Shao, J. Zhao, and Y. Gao, *Mon. Not. Roy. Astron. Soc.* **496**, 182 (2020), [arXiv:2004.12096 \[astro-ph.HE\]](#) .
- [139] S. Datta, A. Gupta, S. Kastha, K. G. Arun, and B. S. Sathyaprakash, *Phys. Rev. D* **103**, 024036 (2021), [arXiv:2006.12137 \[gr-qc\]](#) .
- [140] H. Nakano, R. Fujita, S. Isoyama, and N. Sago, *Universe* **7**, 53 (2021), [arXiv:2101.06402 \[gr-qc\]](#) .

- [141] T. Yang, *JCAP* **05**, 044 (2021), arXiv:2103.01923 [astro-ph.CO] .
- [142] C. Liu and L. Shao, *Astrophys. J.* **926**, 158 (2022), arXiv:2108.08490 [astro-ph.HE] .
- [143] L.-G. Zhu, L.-H. Xie, Y.-M. Hu, S. Liu, E.-K. Li, N. R. Napolitano, B.-T. Tang, J.-d. Zhang, and J. Mei, *Sci. China Phys. Mech. Astron.* **65**, 259811 (2022), arXiv:2110.05224 [astro-ph.CO] .
- [144] Y. Kang, C. Liu, and L. Shao, *Mon. Not. Roy. Astron. Soc.* **515**, 739 (2022), arXiv:2205.02104 [astro-ph.HE] .
- [145] B. C. Seymour, H. Yu, and Y. Chen, *Phys. Rev. D* **108**, 044038 (2023), arXiv:2208.01668 [gr-qc] .
- [146] T. Baker, E. Barausse, A. Chen, C. de Rham, M. Pieroni, and G. Tasinato, *JCAP* **03**, 044 (2023), arXiv:2209.14398 [gr-qc] .
- [147] R. Abbott *et al.* (KAGRA, VIRGO, LIGO Scientific), *Phys. Rev. X* **13**, 011048 (2023), arXiv:2111.03634 [astro-ph.HE] .
- [148] L. Wen and Y. Chen, *Phys. Rev. D* **81**, 082001 (2010), arXiv:1003.2504 [astro-ph.CO] .
- [149] W. Zhao and L. Wen, *Phys. Rev. D* **97**, 064031 (2018), arXiv:1710.05325 [astro-ph.CO] .
- [150] H.-S. Cho, *Class. Quant. Grav.* **32**, 235007 (2015), arXiv:1502.04399 [gr-qc] .
- [151] P. Kumar, T. Chu, H. Fong, H. P. Pfeiffer, M. Boyle, D. A. Hemberger, L. E. Kidder, M. A. Scheel, and B. Szilagyi, *Phys. Rev. D* **93**, 104050 (2016), arXiv:1601.05396 [gr-qc] .
- [152] C. Cutler *et al.*, *Phys. Rev. Lett.* **70**, 2984 (1993), arXiv:astro-ph/9208005 .
- [153] L. Blanchet and B. R. Iyer, *Phys. Rev. D* **71**, 024004 (2005), arXiv:gr-qc/0409094 .
- [154] B. S. Sathyaprakash and B. F. Schutz, *Living Rev. Rel.* **12**, 2 (2009), arXiv:0903.0338 [gr-qc] .
- [155] S. Borhanian, *Class. Quant. Grav.* **38**, 175014 (2021), arXiv:2010.15202 [gr-qc] .
- [156] M. Di Giovanni, C. Giunchi, G. Saccorotti, A. Berbellini, L. Boschi, M. Olivieri, R. De Rosa, L. Naticchioni, G. Oggiano, M. Carpinelli, D. D'Urso, S. Cuccuru, V. Sipala, E. Calloni, L. Di Fiore, A. Grado, C. Migoni, A. Cardini, F. Paoletti, I. Fiori, J. Harms, E. Majorana, P. Rapagnani, F. Ricci, and M. Punturo, *Seismological Research Letters* **92**, 352 (2020).
- [157] S. Kawamura *et al.*, *PTEP* **2021**, 05A105 (2021), arXiv:2006.13545 [gr-qc] .
- [158] P. Jaranowski, A. Krolak, and B. F. Schutz, *Phys. Rev. D* **58**, 063001 (1998), arXiv:gr-qc/9804014 .
- [159] N. Arnaud, M. Barsuglia, M.-A. Bizouard, P. Canitrot, F. Cavalier, M. Davier, P. Hello, and T. Pradier, *Phys. Rev. D* **65**, 042004 (2002), arXiv:gr-qc/0107081 .
- [160] B. F. Schutz, *Class. Quant. Grav.* **28**, 125023 (2011), arXiv:1102.5421 [astro-ph.IM] .
- [161] K. Yagi and N. Seto, *Phys. Rev. D* **83**, 044011 (2011), [Erratum: *Phys.Rev.D* 95, 109901 (2017)], arXiv:1101.3940 [astro-ph.CO] .
- [162] S. Kawamura *et al.*, *Class. Quant. Grav.* **23**, S125 (2006).
- [163] <https://gwosc.org/eventapi/html/GWTC/>.
- [164] S. Hild *et al.*, *Class. Quant. Grav.* **28**, 094013 (2011), arXiv:1012.0908 [gr-qc] .
- [165] <https://cosmicexplorer.org/sensitivity.html>.
- [166] L. S. Finn, *Phys. Rev. D* **46**, 5236 (1992), arXiv:gr-qc/9209010 .
- [167] C. M. Hirata, D. E. Holz, and C. Cutler, *Phys. Rev. D* **81**, 124046 (2010), arXiv:1004.3988 [astro-ph.CO] .
- [168] N. Tamanini, C. Caprini, E. Barausse, A. Sesana, A. Klein, and A. Petiteau, *JCAP* **04**, 002 (2016), arXiv:1601.07112 [astro-ph.CO] .
- [169] B. Kocsis, Z. Frei, Z. Haiman, and K. Menou, *Astrophys. J.* **637**, 27 (2006), arXiv:astro-ph/0505394 .
- [170] E. Barausse, *Mon. Not. Roy. Astron. Soc.* **423**, 2533 (2012), arXiv:1201.5888 [astro-ph.CO] .
- [171] R. Laureijs *et al.* (EUCLID), (2011), arXiv:1110.3193 [astro-ph.CO] .
- [172] D. Spergel *et al.*, (2015), arXiv:1503.03757 [astro-ph.IM] .
- [173] P. A. Abell *et al.* (LSST Science, LSST Project), (2009), arXiv:0912.0201 [astro-ph.IM] .
- [174] v. Ivezić *et al.* (LSST), *Astrophys. J.* **873**, 111 (2019), arXiv:0805.2366 [astro-ph] .
- [175] Y. Cao *et al.*, *Mon. Not. Roy. Astron. Soc.* **480**, 2178 (2018), arXiv:1706.09586 [astro-ph.IM] .
- [176] Y. Cao, Y. Gong, D. Liu, A. Cooray, C. Feng, and X. Chen, *Mon. Not. Roy. Astron. Soc.* **511**, 1830 (2022), arXiv:2108.10181 [astro-ph.CO] .
- [177] Y. Cao, Y. Gong, Z.-Y. Zheng, and C. Xu, *Res. Astron. Astrophys.* **22**, 025019 (2022), arXiv:2110.07088 [astro-ph.CO] .
- [178] Y. Gong, X. Liu, Y. Cao, X. Chen, Z. Fan, R. Li, X.-D. Li, Z. Li, X. Zhang, and H. Zhan, *Astrophys. J.* **883**, 203 (2019), arXiv:1901.04634 [astro-ph.CO] .